Design of Interval Type-2 Fuzzy Controllers for Active Magnetic Bearing Systems

Gui-Ping Ren, *Student Member, IEEE*, Zhiyong Chen, *Senior Member, IEEE*, Hai-Tao Zhang, *Senior Member, IEEE*, Yue Wu, *Member, IEEE*, Haofei Meng, Dongrui Wu, *Senior Member, IEEE*, and Han Ding, *Senior Member, IEEE*

***Abstract*—This article proposes an active levitation control system composed of an active magnetic bearing (AMB) rotor and an interval type-2 (IT2) model-based fuzzy logic controller (FLC). The controller aims to achieve fast and stable levitation by compensating for system uncertainties via proper design of IT2 membership functions. In particular, the complex nonlinear dynamics of the AMB are modeled as a set of local linear systems around multiple operating points, which can be stabilized by a parallel distributed compensation scheme. Sufficient conditions are derived to guarantee the asymptotical stability of the closed-loop system based on the linear matrix inequality approach and the Lyapunov stability theory. Moreover, input constraints are applied in an enhanced version of the controller. Experiments on a real AMB platform were conducted to demonstrate the effectiveness and superiority of the proposed IT2 FLC.**

***Index Terms*—Fuzzy control, magnetic levitation, uncertainty.**

I. Introduction

ACTIVE magnetic bearings (AMBs) are widely used in modern manufacturing and machining processes. They use contactless electromagnetic forces, generated by electromagnetic coils, to support rotors. Compared to conventional mechanical and hydrostatic bearings, AMBs have higher rotational speed, better resistance to external disturbances, and longer operational life span [1]–[4]. Furthermore, with the adjustable currents of electromagnetic coils, both rotor damping and stiffness of AMBs become controllable through an active closed-loop setup, which is highly desirable in industrial manufacturing. From the vibration control point of view, with the assistance of an active controller, AMBs can serve as active excitation absorbers to mitigate chatters of milling processes. Active controller design of AMBs can reduce their cost and increase their efficiency while maintaining the maximal metal-removal rate (MMRR) [5]. Due to all the aforementioned advantages, these years have witnessed numerous applications of AMBs in various industrial fields including renewable energy [6], aerospace [7], machining [3], [4], [8], biomedical industry [9], [10], etc.

Generally speaking, a magnetic levitation spindle contains five degrees of freedom (DOFs), i.e., two radial AMBs and one axial AMB called thrust bearing. Each AMB is a multi-input/multioutput electromechanical integrated nonlinear system with severe couplings which are embedded with position sensors, current amplifiers, electromagnetic actuators (coils), and a levitation controller. For instance, the electromagnetic forces have a typical relationship with current of actuator and displacement of rotor. Thus, it becomes a challenging task to develop a niche intelligent controller to regulate the open-loop unstable nonlinear AMB [11].

Other representative efforts were devoted to the methods using linearization AMB models, such as linear quadratic regulator (LQR) [12], model predictive control (MPC) [13], and sliding mode control [14]. To improve the disturbance rejection capability, researchers developed H_∞ robust control to stabilize a magnetic levitation bearing in the presence of mass imbalance disturbances; see, e.g., [15], [16]. The extended state observer-based controller designed in [17] is based on feedback linearization and the differential geometry theory and it also aims to attenuate extend disturbances. The μ-synthesis robust control proposed in [18] is a unique control law to prevent levitation failure.

Recently, with the emergence of intelligent machining in manufacturing, linear controllers become more incapable of fulfilling the increasing requirements in modern machining industries. Thus, some efforts were devoted to nonlinear and adaptive

Manuscript received July 9, 2019; revised January 3, 2020; accepted February 23, 2020. Date of publication March 3, 2020; date of current version October 14, 2020. Recommended by Technical Editor Y. Shtessel. This work was supported by the National Natural Science Foundation of China under Grant U1713203, Grant 61673189, Grant 51721092, Grant 51729501, Grant 61873321, and Grant 61803168. *(Corresponding authors: Hai-Tao Zhang; Han Ding.)*

Gui-Ping Ren, Hai-Tao Zhang, Yue Wu, and Haofei Meng are with the Key Laboratory of Image Processing and Intelligent Control, School of Artificial Intelligence and Automation and the State Key Laboratory of Digital Manufacturing Equipment and Technology, School of Mechanical Science and Engineering, Huazhong University of Science and Technology, Wuhan 430074, China (e-mail: allenren@hust.edu.cn; zht@mail.hust.edu.cn; wuyue_a@126.com; hfmeng@hust.edu.cn).

Zhiyong Chen is with the School of Electrical Engineering and Computing, The University of Newcastle, Callaghan, NSW 2308, Australia (e-mail: zhiyong.chen@newcastle.edu.au).

Dongrui Wu is with the Key Laboratory of Image Processing and Intelligent Control, School of Artificial Intelligence and Automation, Huazhong University of Science and Technology, Wuhan 430074, China (e-mail: drwu09@gmail.com).

Han Ding is with the State Key Laboratory of Digital Manufacturing Equipment and Technology, School of Mechanical Science and Engineering, Huazhong University of Science and Technology, Wuhan 430074, China (e-mail: dinghan@hust.edu.cn).

Color versions of one or more of the figures in this article are available online at http://ieeexplore.ieee.org.

Digital Object Identifier 10.1109/TMECH.2020.2978018

control schemes to reduce the settling time while maintaining adequate control performance over a sufficiently large operational region. An adaptive switching learning proportional derivative (PD) controller was proposed and implemented for quick trajectory tracking of robot manipulators in [19]. Yuan *et al.* proposed a general framework for the identification of networked systems as well as the inference of dynamics transition and switch logics in [20], and provided a scheme for automatically detecting and localizing faults in manufacturing systems in [21]. With the aid of second-order sliding mode technique, a novel control scheme was proposed in [22] to address system uncertainties and hence, mitigate the influences of harmonic disturbances.

Although these novel nonlinear AMB controllers have shown potential in real-world machining processes, most of them require a highly matched dynamics model, which suffers from various system uncertainties [23], given as follows.

1) *Assembly uncertainty:* Mismatch between the geometric and physical centers, leading to parameter uncertainties of the coil-sensor angle and the air gap.
2) *Actuator uncertainty:* Self-/mutual-inductance effects of actuator dynamics, leading to uncertainties of magnetic forces.
3) *Environmental noises:* Environmental noise, inducing unexpected vibrations and measurement noise.

Furthermore, the existence of the nonlinear Lorentz force intensifies the challenge of the AMB control to achieve stable and desired levitation performance. These inevitably hinder the further applications of existing nonlinear controllers.

To address these complex uncertainties and nonlinearities in AMB dynamics, some scholars sought assistance from intelligent or heuristic control schemes such as Takagi–Sugeno (T–S) fuzzy control which rely much less on an accurate nonlinear model than the conventional approaches [24]. For example, a T–S fuzzy controller was developed in [25] for magnetic bearings with high-speed motors. Afterward, a type-1 (T1) fuzzy logical controller was combined with genetic algorithm (GA) and moth-flame optimization (MFO) to achieve precise and fast levitation for AMBs [26], [27]. However, it is arduous to tune the parameters of optimal fuzzy sets (FSs) in these optimization algorithms and the computational cost remains a practical issue. As a remedy, the type-2 FS control was later adapted to handle more uncertainties than T1 FSs.

The initial type-2 fuzzy logic controllers (FLCs) usually consume too many computing resources [28], and hence, their researches and applications are limited in practice. Interval type-2 (IT2) FLC is a simplification of T2 FLCs, whose membership is an interval instead of conventional T1 FS and the operational process is faster [29], [30]. For instance, an IT2 FLC was used in [31] to stabilize and underactuate a mobile two-wheeled inverted pendulum. Recently, IT2 FLCs have attracted more attention and found many successful applications in [32]–[34], among others.

To overcome the assembly error and the nonlinearity of the displacement sensor in AMB systems, we develop a feedback levitation control system composed of coil amplifiers, magnetic displacement sensors, and a dSPACE real-time control hardware equipped with a model-based IT2 FLC. By this means, both the

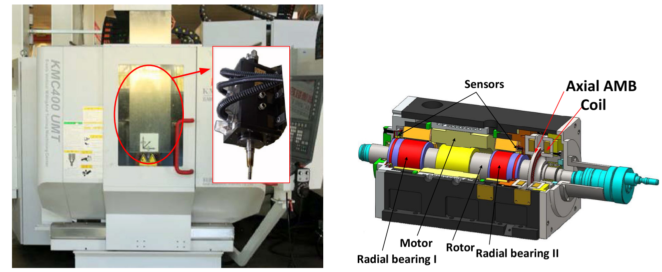

(a) (b)

Fig. 1. (a) Layout and (b) structure of the AMB in a spindle.

control precision and the transient performance can be substantially improved, which is the main technical contribution of the present work. Meanwhile, sufficient conditions are revealed with the assistance of Lyapunov stability theory [35] to guarantee the stability of the closed-loop system using the linear matrix inequality (LMI) approach. The developed control system is expected to find a new practical application of the IT2 fuzzy theory and the T–S fuzzy control method in manufacturing and machining industries.

The rest of this article is organized as follows. Section II introduces the active levitation control platform and the dynamics of the AMB system. Section III proposes an IT2 T–S model-based FLC for the nonlinear AMB system. Section IV presents the stability analysis to derive the asymptotical stability conditions. Section V describes extensive AMB levitation experiments to demonstrate the effectiveness and advantages of the proposed IT2 FLC. Finally, Section VI concludes this article.

Throughout the article, the notations "$\prec$" ("$\preceq$") and "$\succ$" ("$\succeq$") denote negative (nonnegative) and positive (semipositive) definiteness of square matrices, respectively. The operator "$\otimes$" represents the Kronecker product.

II. System Description and Dynamic Model

The equipment layout and the structure of the experimental AMB are depicted in Fig. 1(a) and (b), respectively. The control system for a five-axis magnetic levitation spindle illustrated in Fig. 2 consists of ten-channel current drive loops. The control loop of each axis is composed of a magnetic bearing, a digital controller, two current amplifiers, two opposing electromagnetic coils, and a displacement sensor with a signal adjust circuit.

The displacement of the bearing in each loop (i.e., the output y) in Fig. 2 is detected by the position sensor and converted to an analog voltage signal. Afterward, the analog signal is sampled to a digital one by the analog-digital (AD) converter and then, fed into the controller, where the control current is calculated and amplified to drive the coil of the loop. In this way, the position of the AMB is regulated by online active magnetic forces. The essential part of the AMB under investigation is the radial eight-pole bearing with the two coil pairs as shown in Fig. 3.

As shown in Fig. 2, the AMB spindle is customized by Foshan Genesis AMB (FG-AMB) Technology Comapny Ltd. The control law is implemented by a dSPACE1103 module with

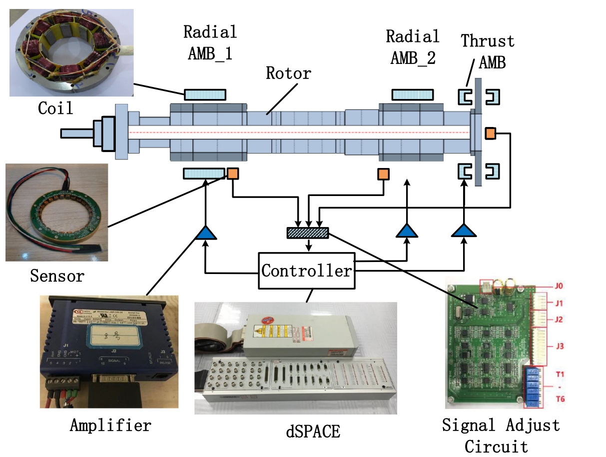

Fig. 2. Hardware architecture of the control system of a magnetic levitation spindle.

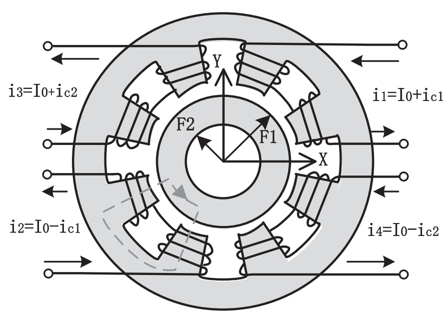

Fig. 3. Eight-pole structure of a radial AMB with two coil pairs.

multichannel high-precision AD/DA convertors. Each actuator of the AMB consists of current amplifiers and electromagnetic coils. The current driver amplifiers are Jsp-180-20 of Junus Servoamplifier. Each coil is regarded as the inductive load with an inductance L and resistance R. Therein, the embedded current driving amplifiers are equipped with PI controller to guarantee the highly efficient current control response. The voltage-amplifier current dynamics are considered to be independent of each other and described as follows [36]:

$$\ddot{i}_\ell + 2\zeta_\ell\omega_\ell\dot{i}_\ell + \omega_\ell^2 i_\ell = \omega_\ell^2 u_\ell \tag{1}$$

where $\ell = 1, 2, 3, 4$ means the sequential number of each coil; u_ℓ and i_ℓ denote the control signal and the output current, respectively; and ζ_ℓ and ω_ℓ are the system coefficients of the actuators. Taking the coil $\ell = 1$ as an example, we generate a series of sinusoidal inputs of different frequencies, and measure the responses of coil current by a Hall current sensor. Then, we can obtain a Bode diagram to identify the parameters ζ_1 and ω_1 shown in Fig. 4, which expresses the relationship between the input and the output of the current loop.

Each sensor of the AMB, also called an inductive displacement transducer, is able to detect the displacement of a bearing. The so-called signal adjust circuit is indispensable to provide power for the sensors and process the initial measurement signal. More specifically, it is driven by $J0$ connected to a $\pm$15-V

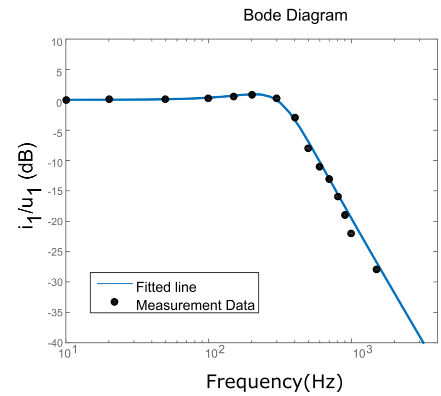

Fig. 4. Identification of the coil current dynamics (1).

voltage source and supplies the sensor and acquires the displacement signals via the interface $J1$. It is worth mentioning that the measured displacement signals inevitably suffer from high-frequency environmental electromagnetic noises. Thus, a low-pass filter circuit is embedded as an essential part of the signal processing module. Finally, by adjusting the slide rheostats $T1 - T6$, the signal adjust circuit after sensor calibration can offer the controller analog signals with a linear gain $Ks = 10\,\text{mV}/\mu\text{m}$ and linearity of 5% for all the displacement sensors in the range of $\pm 250\,\mu$m.

The main objective of the research is to develop an active controller for the levitation process of the vertically placed radial magnetic bearing. We first derive a dynamic model of the eight-pole heteropolar-type radial magnetic bearing depicted in Fig. 3. For simplicity, we assume that all the magnetic fluxes pass through the bearing core and the iron magnetization is ignored. The four independent and symmetric coils are orthogonal to the X–Y sensors. Accordingly, the electromagnetic force and the rotor position in the X and Y directions are decoupled [1]. This is the advantage of the structure of eight-pole bearings over other types, such as three-pole unipolar bearings. Specifically, in Fig. 3, i_ℓ and $i_{c\ell}$ represent the command and the control currents of electromagnet coils with bias currents I_0, respectively. Besides, F_1 and F_2 denote the forces yielded by the two pairs of cross-electromagnetic coil actuators, respectively.

Due to the directional difference between the outputs (i.e., the displacements x and y) and inputs (i.e., F_x and F_y), it is necessary to transfer the detected X- and Y- displacements x_m and y_m to the real displacements x and y as follows:

$$\begin{bmatrix} x \\ y \end{bmatrix} = \frac{\sqrt{2}}{2}\begin{bmatrix} 1 & 1 \\ -1 & 1 \end{bmatrix}\begin{bmatrix} x_m \\ y_m \end{bmatrix}$$
$$\text{s.t. } |x| \le x_{\max} \quad |y| \le y_{\max}.$$

Here, $x_{\max} = y_{\max} = l_0/2$ is the auxiliary gap distance of the backup bearing, and l_0 is the distance of the nominal air gap between the centering rotor and the electromagnet.

By the Maxwell field theorem [37], the magnetic force of an electromagnetic coil is

$$F(x,i) = \frac{\mu A}{4}\frac{(2Ni)^2}{(l_0-x)^2}\cos\frac{\beta}{2} = k\frac{i^2}{(l_0-x)^2}$$
$$k = \mu A N^2 \cos\frac{\beta}{2} \tag{2}$$

where i is the current of the coil, A represents the pole area, N is the number of the winding pole turns, μ denotes the air (approximately vacuum) permeability, i.e., $\mu \approx \mu_0 = 4\pi e^{-7}$Vs/Am, and $\beta = \pi/4$ is the angle between each pair of adjacent poles. Specifically, the cross coupling forces for the X and Y axes are, respectively

$$F_x(x,i_{c1}) = F_{i1} - F_{i3} = k\frac{(I_0+i_{c1})^2}{(l_0-x)^2} - k\frac{(I_0-i_{c1})^2}{(l_0+x)^2}$$
$$F_y(y,i_{c2}) = F_{i2} - F_{i4} = k\frac{(I_0+i_{c2})^2}{(l_0-y)^2} - k\frac{(I_0-i_{c2})^2}{(l_0+y)^2}. \tag{3}$$

The AMB works in the same way in each axis and obeys the same dynamics. For example, the displacement in the X axis follows Newton's second law $m\ddot{x} = F_x(x,i_{c1})$. Let us specify $r > 1$ nominal positions $x_i^*, i = 1,\ldots,r$. Around each working point $(x,i_c) = (x_i^*,0)$, the dynamics can be linearized as follows:

$$\ddot{x} = \frac{F_x(x,i_{c1})|_{(x^*,0)}}{m} = a_i(x-x_i^*) + b_i i_{c1} + c_i \tag{4}$$

with

$$a_i = \frac{2kI_o^2}{m}\left[\frac{1}{(l_0-x_i^*)^3} + \frac{1}{(l_0+x_i^*)^3}\right]$$
$$b_i = \frac{2kI_0}{m}\left[\frac{1}{(l_0-x_i^*)^2} + \frac{1}{(l_0+x_i^*)^2}\right]$$
$$c_i = \frac{kI_o^2}{m}\left[\frac{1}{(l_0-x_i^*)^2} - \frac{1}{(l_0+x_i^*)^2}\right].$$

Here, we particularly select $r = 5$ and

$$x_1^* = -\frac{l_0}{2} \quad x_2^* = -\frac{l_0}{4} \quad x_3^* = 0 \quad x_4^* = \frac{l_0}{4} \quad x_5^* = \frac{l_0}{2}.$$

It is noted that the coefficients a_i, b_i, and c_i depend on x_i^*. Also, they are radially symmetric about x_i^* due to the specific structure of AMB.

Moreover, denote the state $\mathbf{x} := [x\ \dot{x}]^T$ and the input $u = i_{c1}$. Then, the system (4) can be rewritten into a general state-space model, for $i = 1,\ldots,r$

$$\dot{\mathbf{x}} = A_i\mathbf{x} + B_i u + \varPsi_i \tag{5}$$

where

$$A_i = \begin{bmatrix} 0 & 1 \\ a_i & 0 \end{bmatrix} \quad B_i = \begin{bmatrix} 0 \\ b_i \end{bmatrix} \quad \varPsi_i = \begin{bmatrix} 0 \\ \psi_i \end{bmatrix}$$

and

$$\psi_i = c_i - a_i x_i^* = 16\frac{kI_0^2 l_0}{m}\left[\frac{x_i^*}{l_0^2 - (x_i^*)^2}\right]^3.$$

Here, ψ_i represents an offset force relative to position. For example, $\psi_3 = 0$ associated with $x_3^* = 0$ and $\psi_1 = -(128kI_0^2)/(27ml_0^2)$ associated with $x_1^* = -l_0/2$. The nonzero ψ_1 means that the nonnegligible additional force needs to be compensated by a current $-\psi_1/b_1 = 8I_0/15$ from (5).

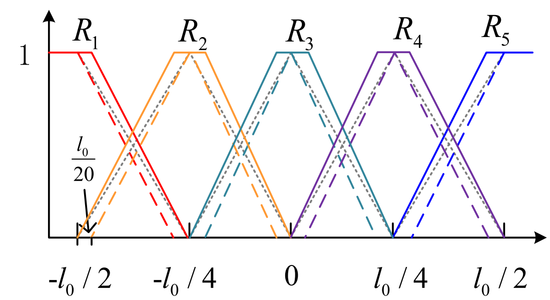

Fig. 5. Profile of fuzzy membership functions. Solid lines, dashed lines, and spotted lines are UMFs, LMFs, and T1 fuzzy MFs, respectively.

III. IT2 FLC Design

In this section, we appeal to the T–S fuzzy model [38] to deal with the severe nonlinearities of the AMB's dynamic (5) noting that the matrices A_i, B_i, and Φ_i depend on x_i^*. Specially, for each $x_i^*, i = 1,\ldots,r$, the ith local rule of the T–S model is

$$\begin{aligned}\text{Rule } i:\ &\text{If } x \text{ is } M^i\\ &\text{then } \dot{\mathbf{x}} = A_i\mathbf{x} + B_i u + \Psi_i\end{aligned} \tag{6}$$

where M^i represents the FS in the domain around x_i^*. The second line in (6) is from (5) and is called a local subsystem.

For a conversional T1 T–S model, the fuzzy membership functions for the FSs M^i, $i = 1,\ldots,r$, are plotted in dotted lines in Fig. 5. In this article, to deal with the nonlinear uncertainties more adequately, we adopt the so-called IT2 T–S fuzzy model [39], where each FS $\widetilde{M}^i$ has two fuzzy membership functions, called the upper membership functions (UMFs) and the lower membership functions (LMFs). In particular, they are plotted in solid and dashed lines in Fig. 5, respectively. The UMFs and LMSs, denoted by $\bar{\omega}_i$ and $\underline{\omega}_i$, write

$$R_{1,5}: \bar{\omega}_1(-x) = \bar{\omega}_5(x) := \begin{cases} \frac{x-l_0/4}{l_0/5} & \frac{l_0}{4} < x < \frac{9l_0}{20} \\ 1 & x \geq \frac{9l_0}{20} \\ 0 & \text{otherwise} \end{cases}$$
$$\underline{\omega}_1(-x) = \underline{\omega}_5(x) := \begin{cases} \frac{x-3l_0/10}{l_0/5} & \frac{3l_0}{10} < x < \frac{l_0}{2} \\ 1 & x \geq \frac{l_0}{2} \\ 0 & \text{otherwise} \end{cases} \tag{7}$$
$$R_{2,4}: \bar{\omega}_2(-x) = \bar{\omega}_4(x) := \begin{cases} \frac{x}{l_0/5} & 0 < x < \frac{l_0}{5} \\ 1 & \frac{l_0}{5} \leq x \leq \frac{3l_0}{10} \\ \frac{l_0/2-x}{l_0/5} & \frac{3l_0}{10} < x < \frac{l_0}{2} \\ 0 & \text{otherwise} \end{cases}$$

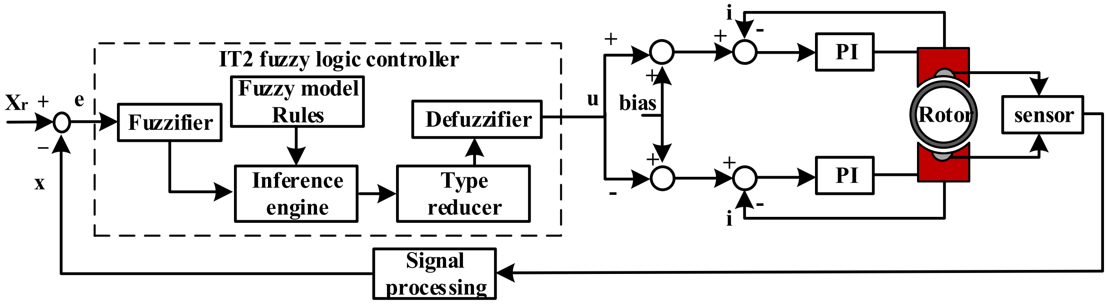

Fig. 6. Structure of the IT2 FLC on AMB system.

$$\underline{\omega}_2(-x) = \underline{\omega}_4(x) := \begin{cases} \frac{x - l_0/20}{l_0/5} & \frac{l_0}{20} < x < \frac{l_0}{4} \\ 1 & |x| = \frac{l_0}{4} \\ \frac{9l_0/20 - x}{l_0/5} & \frac{l_0}{4} < x < \frac{9l_0}{20} \\ 0 & \text{otherwise} \end{cases} \tag{8}$$

$$R_3 : \underline{\omega}_3(x) := \begin{cases} 1 & -l_0/20 \le x \le l_0/20 \\ \frac{l_0/4 - |x|}{l_0/5} & l_0/20 < |x| < l_0/4 \\ 0 & \text{otherwise} \end{cases}$$

$$\underline{\omega}_3(x) := \begin{cases} \frac{l_0/5 - |x|}{l_0/5} & |x| < l_0/5 \\ 0 & \text{otherwise}. \end{cases} \tag{9}$$

Accordingly, with the aforementioned fuzzy rules, the overall IT2 T–S model can be written as follows:

$$\dot{\mathbf{x}} = \sum_{i=1}^{r} \omega_i(x)(A_i\mathbf{x} + B_i u + \Psi_i) \tag{10}$$

where the sequential function $\omega_i(x)$ is selected between the UMF $\bar{\omega}_i(x)$ and the LMF $\underline{\omega}_i(x)$. The function ω_i is solved by the Nie–Tan method [40], [41]

$$\omega_i(x) = \alpha\underline{\omega}_i(x) + (1-\alpha)\overline{\omega}_i(x)$$
$$\text{subject to } \sum_{i=1}^{r} \omega_i(x) = 1 \tag{11}$$

with $\alpha = 0.5$.

The controller has two components for feedback stabilization and feedforward compensation, represented by

$$u = u^{\text{fb}} + u^{\text{ff}}. \tag{12}$$

Inspired by the parallel distributed compensation (PDC), the fuzzy logic feedback controller is of the form

$$\begin{aligned} &\text{Rule } i: \text{ If } x \text{ is } \widetilde{M}^i \\ &\quad\text{then } u = -K_i\mathbf{x} \end{aligned} \tag{13}$$

with the local feedback gains K_i, $i = 1, \ldots, 5$ to be designed to stabilize the local linear system (A_i, B_i). Using the same algorithm as (11), the defuzzified output of (13) is

$$u^{\text{fb}} = -\sum_{i=1}^{r} \omega_i(x)K_i\mathbf{x}. \tag{14}$$

Also, the feedforward compensation can be designed as

$$u^{\text{ff}} = -\frac{\sum_{i=1}^{r}\omega_i(x)\psi_i}{\sum_{i=1}^{r}\omega_i(x)b_i} \tag{15}$$

to account for the offset force in the model (5).

Remark 1: The structure of the proposed controller (12) is shown in Fig. 6. An IT2 FLC consists of an IT2 fuzzifier, a rulebase, an inference engine, a type-reducer, and a defuzzifier. The main difference between an IT2 FLC and a T1 FLC is the type-reducer, by which the former output of the inference engine based on an IT2 FS is converted into a T1 FS. Afterward, conventional defuzzification can be performed. Specially, the footprint of uncertainty (FOU) of an IT2 FS provides an extra degree of freedom, which endows the capability to handle more uncertainties of experiential fuzzy rules [42].

IV. Stability Analysis

Now, we will give the main theoretical result assuring the stability of the closed-loop system composed of (10), (12), (14), and (15).

Theorem 1: The close-loop system composed of (10), (12), (14), and (15) is globally asymptotically stable, if there exist symmetric real matrix $P \succ 0$ and W such that

$$\begin{cases} \Phi_{i,i} + W_{i,i} \prec 0 \\ \Phi_{i,j} + W_{i,j} \preceq 0 \\ \Delta \succ 0 \end{cases} \tag{16}$$

with

$$\Delta = \begin{bmatrix} W_{1,1} & W_{1,2} & & \mathbf{0} \\ W_{21} & W_{2,2} & \ddots & \\ & \ddots & \ddots & W_{r-1,r} \\ \mathbf{0} & & W_{r,r-1} & W_{r,r} \end{bmatrix}$$

for

$$\Phi_{i,j} = G_{i,j}^T P + PG_{i,j}, \; G_{i,j} = A_i - B_i K_j, \quad i,j = 1, \ldots, r.$$

Proof: First of all, the system composed of (10), (12), and (14) can be rewritten as follows:

$$\begin{aligned}\dot{\mathbf{x}} &= \sum_{i=1}^{r}\omega_i(x)(A_i\mathbf{x} + B_i u^{\text{fb}} + B_i u^{\text{ff}} + \Psi_i)\\ &= \sum_{i=1}^{r}\omega_i(x)(A_i\mathbf{x} - B_i\sum_{j=1}^{r}\omega_j(x)K_j\mathbf{x} + B_i u^{\text{ff}} + \Psi_i)\\ &= \sum_{i=1}^{r}\sum_{j=1}^{r}\omega_i(x)\omega_j(x)(A_i - B_iK_j)\mathbf{x}\\ &\quad + \sum_{i=1}^{r}\omega_i(x)(B_i u^{\text{ff}} + \Psi_i)\end{aligned}$$

where $\sum_{j=1}^{r}\omega_j(x) = 1$ is used in the last equation. From (15), one has

$$\sum_{i=1}^{r}\omega_i(x)(B_i u^{\text{ff}} + \Psi_i) = 0.$$

As a result, the closed-loop system becomes

$$\dot{\mathbf{x}} = \sum_{i=1}^{r}\sum_{j=1}^{r}\omega_i(x)\omega_j(x)G_{i,j}\mathbf{x}. \tag{17}$$

Now, define a Lyapunov function candidate

$$V(\mathbf{x}) = \mathbf{x}^T P\mathbf{x} \tag{18}$$

whose temporal derivative along the trajectory of the closed-loop system (17) satisfies

$$\begin{aligned}\dot{V}(\mathbf{x}) &= \dot{\mathbf{x}}(t)^T P\mathbf{x}(t) + \mathbf{x}(t)^T P\dot{\mathbf{x}}(t)\\ &= \sum_{i=1}^{r}\sum_{j=1}^{r}\omega_i(x)\omega_j(x)\mathbf{x}^T\Phi_{i,j}\mathbf{x}\\ &= (\omega(x)\otimes\mathbf{x})^T\bar{\Phi}(\omega(x)\otimes\mathbf{x})\\ &\le -\sum_{i=1}^{r}\sum_{j=1}^{r}\omega_i(x)\omega_j(x)\mathbf{x}^T W_{i,j}\mathbf{x}\\ &= -(\omega(x)\otimes\mathbf{x})^T\bar{\Delta}(\omega(x)\otimes\mathbf{x})\end{aligned}$$

for

$$\omega(x) = [\omega_1(x),\ldots,\omega_r(x)]^T$$

$$\bar{\Phi} = \begin{bmatrix}\Phi_{1,1} & \Phi_{1,2} & \cdots & \Phi_{1,r}\\ \Phi_{2,1} & \Phi_{2,2} & \ddots & \vdots\\ \vdots & \ddots & \ddots & \Phi_{r-1,r}\\ \Phi_{r,1} & \cdots & \Phi_{r,r-1} & \Phi_{r,r}\end{bmatrix}$$

$$\bar{\Delta} = \begin{bmatrix}W_{1,1} & W_{1,2} & \cdots & W_{1,r}\\ W_{2,1} & W_{2,2} & \ddots & \vdots\\ \vdots & \ddots & \ddots & W_{r-1,r}\\ W_{r,1} & \cdots & W_{r,r-1} & W_{r,r}\end{bmatrix}.$$

Bearing in mind the fuzzy membership functions in Fig. 5 and the criterion (11), one has

$$\begin{aligned}&\omega_i(x)\omega_j(x) = 0 \quad \forall i,j = 1,\ldots,r, |i-j|\ge 2\\ &\omega_i(x) + \omega_{i+1}(x) = 1 \quad \forall i = 1,\ldots,r-1.\end{aligned}$$

Therefore, one has

$$(\omega(x)\otimes\mathbf{x})^T\bar{\Delta}(\omega(x)\otimes\mathbf{x}) = (\omega(x)\otimes\mathbf{x})^T\Delta(\omega(x)\otimes\mathbf{x})$$

$$\|\omega(x)\|^2 = \sum_{i=1}^{r}\omega_i^2(x) \ge 0.5.$$

As a result

$$\begin{aligned}\dot{V}(\mathbf{x}) &\le -\lambda_{\min}(\Delta)\|\omega(x)\otimes\mathbf{x}\|^2\\ &= -\lambda_{\min}(\Delta)\|\omega(x)\|^2\|\mathbf{x}\|^2\\ &\le -0.5\lambda_{\min}(\Delta)\|\mathbf{x}\|^2\end{aligned}$$

where $\lambda_{\min}(\Delta) > 0$ is the minimum eigenvalue of $\Delta \succ 0$. It concludes that the close-loop system is globally asymptotically stable. ■

Remark 2: The feedback gain K_i for each local subsystem (A_i, B_i) can be calculated via the LQR method by choosing appropriate positive factors $0 < \lambda_1, \lambda_2 < 1/x_{\max}^2$ and $0 < \delta < 1/u_{\max}^2$ for the weighted matrixes $Q = \text{diag}(\lambda_1,\lambda_2)$, $R = \delta I$. Here, $x_{\max}$ and $u_{\max}$ are two specified bounds. In particular, $u_{\max}$ is the saturation threshold of the controller. Referring to the cost function $J = \frac{1}{2}\int(\mathbf{x}^T Q\mathbf{x} + u^T Ru)dt$, one can use an off-line search algorithm to find out the three factors such that the solution K_i satisfies the condition (16).

Remark 3: From the proof of Theorem 1, it is easy to see that the statement still holds if the LMI condition (16) is replaced by $\bar{\Phi} \prec 0$. However, the former is less conservative, thanks to the properties of the adopted IT2 fuzzy memberships. There are some other stability conditions for the fuzzy controller, such as the three equivalent conditions derived by considering the fuzzy logic system as an uncertain system in [43]. However, due to the severe nonlinearities of the AMB system (5), the LMI conditions used in [43] are not suitable here.

Next, we will consider the practical air gap of the bearings as well as the control input constraints. In particular, it is required that $\|\mathbf{x}(t)\| \le x_{\max}$ and $|u(t)| \le u_{\max}$ hold for all time $t \ge 0$ for two specified constants $x_{\max}$ and $u_{\max}$. The result is stated in the following corollary.

Corollary 1: Denote a constant

$$u_{\max}^{\text{ff}} = \max_{\omega_i \text{ in } (11)}\left|\sum_{i=1}^{r}\omega_i\psi_i\right| / \left|\sum_{i=1}^{r}\omega_i b_i\right| > 0.$$

Pick two positive constants $x_{\max} > 0$ and $u_{\max}^{\text{fb}} > 0$, and hence, $u_{\max} = u_{\max}^{\text{fb}} + u_{\max}^{\text{ff}}$. Suppose the gains K_i, $i = 1,\ldots,r$, satisfy the following LMI:

$$\begin{cases} Q_s \succeq x_{\max}^2 I\\ \begin{bmatrix}\frac{(u_{\max}^{\text{fb}})^2}{x_{\max}^2}I & K_i^T\\ K_i & I\end{bmatrix} \succeq 0\end{cases} \tag{19}$$

TABLE I
AMB ROTOR PARAMETERS

Parameter	Value	Unit
Rotor mass m	6	kg
Winding inductance L	138	mH
Winding resistance R	2	Ω
Nominal air gap l_0	0.50	mm
Auxiliary gap $x_{\max}$	0.25	mm
Bias current I_0	1	A
Coil turns N	180	-
Pole area A	850	mm^2

with $Q_s = P^{-1}$. Then, Theorem 1 holds with

$$\|\mathbf{x}(t)\| \le x_{\max} \quad |u(t)| \le u_{\max}\ \forall t \ge 0.$$

Proof: Using the Schur complement theorem [44], the LMIs (19) are equivalent to

$$Q_s^{-1} = P \le \frac{1}{x_{\max}^2} I \tag{20}$$

$$K_i^T K_i \le \frac{(u_{\max}^{\mathrm{fb}})^2}{x_{\max}^2} I. \tag{21}$$

Substituting (20) into (18) yields

$$\mathbf{x}_0^T P \mathbf{x}_0 \le \tfrac{1}{x_{\max}^2} \mathbf{x}_0^T I \mathbf{x}_0 \le 1. \tag{22}$$

With (21), one has

$$\begin{aligned}
\|u\|^2 &= \sum_{i=1}^{r}\sum_{j=1}^{r} \omega_i\omega_j \mathbf{x}^T K_i^T K_j \mathbf{x} + (u_{\max}^{\mathrm{ff}})^2 + 2u_{\max}^{\mathrm{ff}} \sum_{i=1}^{r} \omega_i K_i \mathbf{x}\\
&\le \sum_{i=1}^{r}\sum_{j=1}^{r} \frac{1}{2}(\omega_i^2+\omega_j^2)\cdot\frac{1}{2}\mathbf{x}^T(K_i^T K_i + K_j^T K_j)\mathbf{x}\\
&\quad + (u_{\max}^{\mathrm{ff}})^2 + 2u_{\max}^{\mathrm{ff}} u_{\max}^{\mathrm{fb}}\\
&\le \sum_{i=1}^{r} \omega_i^2 \mathbf{x}^T K_i^T K_i \mathbf{x} + (u_{\max}^{\mathrm{ff}})^2 + 2u_{\max}^{\mathrm{ff}} u_{\max}^{\mathrm{fb}}\\
&\le \frac{u_s^2}{x_{\max}^2} \sum_{i=1}^{r} \omega_i^2 \mathbf{x}^T I \mathbf{x} + (u_{\max}^{\mathrm{ff}})^2 + 2u_{\max}^{\mathrm{ff}} u_{\max}^{\mathrm{fb}}\\
&\le (u_{\max}^{\mathrm{fb}})^2 + (u_{\max}^{\mathrm{ff}})^2 + 2u_{\max}^{\mathrm{ff}} u_{\max}^{\mathrm{fb}}\\
&= (u_{\max}^{\mathrm{fb}} + u_{\max}^{\mathrm{ff}})^2 \le u_{\max}^2.
\end{aligned} \tag{23}$$

The proof is thus completed. ∎

V. EXPERIMENTS

We apply the developed IT2 T–S fuzzy control law (12) to realize the front bearing's levitation processes of the AMB equipment depicted in Figs. 1 and 2 with the controller structure illustrated in Fig. 6 and the rotor parameters summarized in Table I. The internal model of the fuzzy controller is derived from the symmetric X–Y axes dynamics of the AMB, whose coefficients of (6) are identified as

$$a_1 = a_5 = \frac{16.58k_m}{l_0} \qquad b_1 = b_5 = \frac{8.88k_m}{I_0}$$

$$a_2 = a_4 = \frac{5.76k_m}{l_0} \qquad b_2 = b_4 = \frac{4.82k_m}{I_0}$$

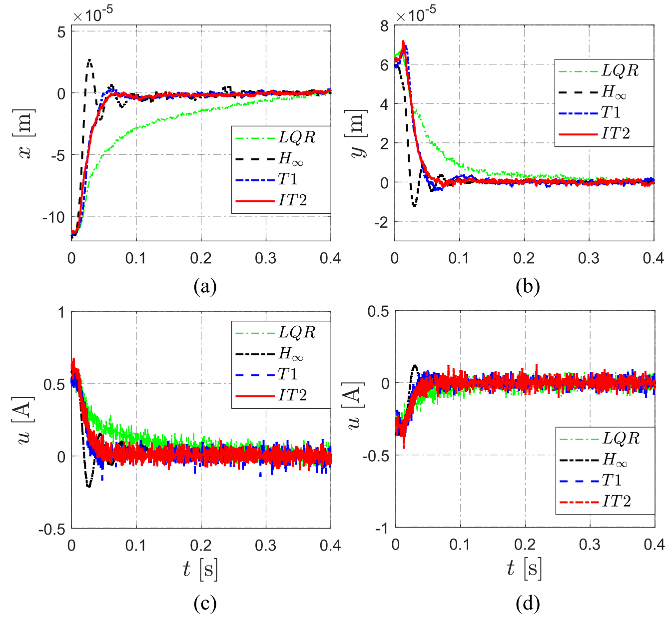

Fig. 7. Evolution of the (a) x-axis and (b) y-axis independent levitation control performance, and (c) and (d) control signals of LQR, H_∞, T1, and IT2 controllers.

$$\psi_1 = -\psi_5 = 4.74k_m \qquad \psi_2 = -\psi_4 = 0.303k_m$$

$$a_3 = \frac{4k_m}{l_0} \qquad b_3 = \frac{4k_m}{I_0}\psi_3 = 0 \tag{24}$$

with $k_m := \frac{kI_0^2}{ml_0^2}$. The IT2 fuzzy sets are designed as (7)–(9) and the sampling time is set as $T_s = 0.1$ ms.

According to (16) of Theorem 1, we can pick the state feedback gains $K_1 = K_5 = [8004, 8.9]$, $K_2 = K_4 = [4771, 9.3]$, and $K_3 = [4002, 9.4]$ for the designed IT2 fuzzy controller (13) by LQR. Hence, we calculate the matrixes P and W by the LMI function of MATLAB and the values are expressed in Appendix.

To verify the advantages of the proposed method, we give the control performance comparison among the proposed IT2 fuzzy law (12) and (15) (in abbr. IT2), the routine T1 fuzzy law (in abbr. T1), the H_∞ controller [16] shown in Appendix (in abbr. H_∞), and the conventional LQR method (in abbr. LQR) in Fig. 7. Therein, the AMB is levitated from the initial position $x = -123\,\mu$m, $y = 64\,\mu$m to the target position $x = 0\,\mu$m, $y = 0\,\mu$m. It is observed that, compared to LQR, the settling time of IT2 is decreased by more than 62% (i.e., from 300 to 114 ms), which implies a significantly accelerated levitation procedure. This is desirable in real applications. From Fig. 5, it is observed from Fig. 8 that the tracking error by IT2 is reduced by 22% in comparison with the fuzzy control law based on the second-order fuzzy membership functions. Although H_∞ fulfills the AMB levitation, its 23.2% overshot is much greater than the proposed method.

To demonstrate the capability of disturbance rejection of the proposed method, we deliberately introduce an external impact disturbance on the bias current at the 0.16th second. Specifically, I_0 of one coil abruptly changes from 1 to 1.5 A lasting 16 sampling periods (1.6 ms). The results in Fig. 9 demonstrate

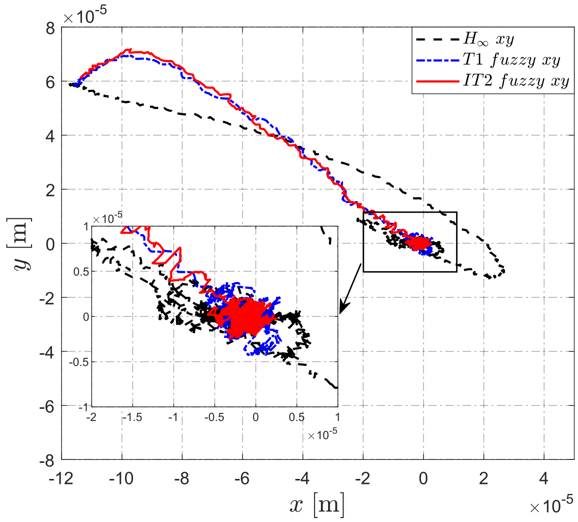

Fig. 8. Comparison of the levitation trajectories of H_∞, T1, and IT2 in the x–y plane.

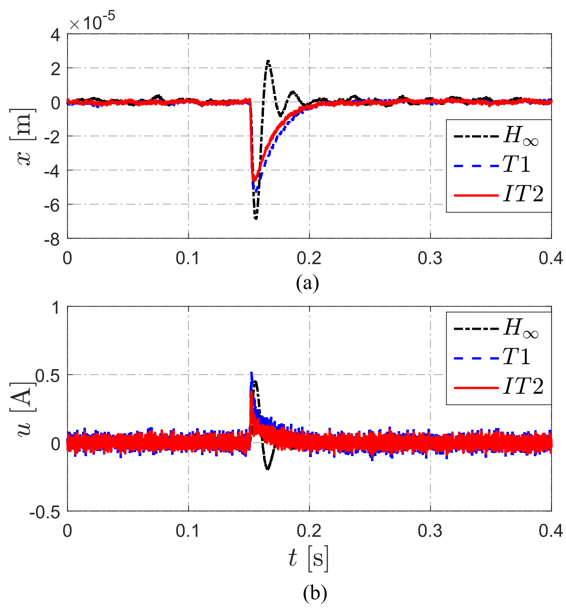

Fig. 9. (a) Evolution of levitation of H_∞, T1, and IT2 and (b) corresponding control signals. Here, an impact on one I_0 from 1 to 1.5 A is introduced at the 0.16th second and lasts for 1.6 ms.

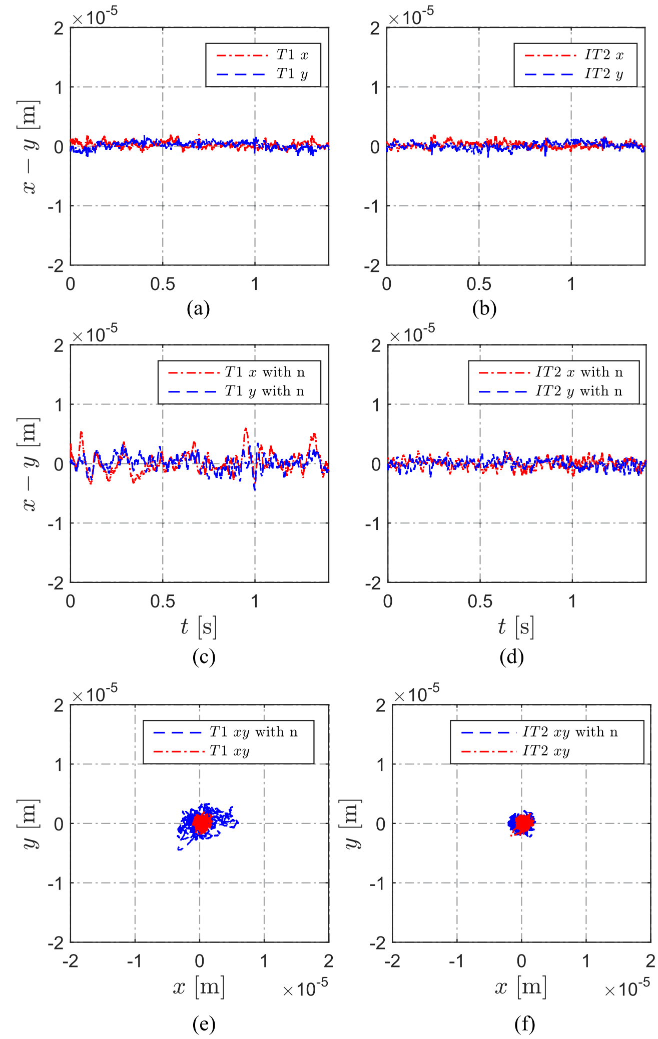

Fig. 10. Comparison of control performance between T1 and IT2 in the x, y-axes: (a) and (b) noise-free case; (c) and (d) case with additional Gaussian noise; (e) and (f) levitation trajectories.

the advantage of IT2 over T1 and H_∞ in terms of restoration from interference.

To show the capability of dealing with external noises, we add random Gaussian noises with mean absolute error $\mathrm{MAE}(n) = 0\,\mu$m and $\mathrm{SD}(n) = 2\,\mu$m to the output displacement signals as shown in Fig. 10. Before adding the noise, the magnitude of the oscillations (quantified by MAE) of IT2 is 22.2% less than that of T1, i.e., 0.9 μm versus 0.7 μm as shown in Fig. 10(a) and (b). After attaching the addition of the noise, the MAE of the feedback displacements IT2 is 36% (i.e., from 2.08 μm to 1.32 μm) less than T1 as shown in Fig. 10 (c) and (d). In other words, the former has a better ability to resist external measurement noises.

To show the advantages of IT2 over T1, we demonstrate the levitation trajectories of both methods as shown in Fig. 10(e) and (f). Therein, all the conditions are the same as Fig. 10 (a)–(d). It is observed that the tracking error area of T1 has been reduced by more than 40% by IT2. Such advantages lie in the fact that the second-order fuzzy membership functions of IT2 in Fig. 5 endow itself superior robustness than the first-order ones in T1. The feasibility and superiority of the proposed IT2 are thus both verified.

What is more, to consider the constraints of control inputs, we make a comparison between the feedback gains based on Theorem 1 (in abbr. T) and the new gains $K_1 = K_5 = [3850,\ 9.5]$, $K_2 = K_4 = [3500,\ 9.3]$, and $K_3 = [3000,\ 9]$ which satisfy (19) of Corollary 1 (in abbr. C). As shown in Fig. 11(a), beginning with the initial point $x = -248.7\,\mu$m, the levitation process of the IT2 fuzzy controller based on Theorem 1 is much faster than that based on Corollary 1. However, Fig. 11(b) shows that

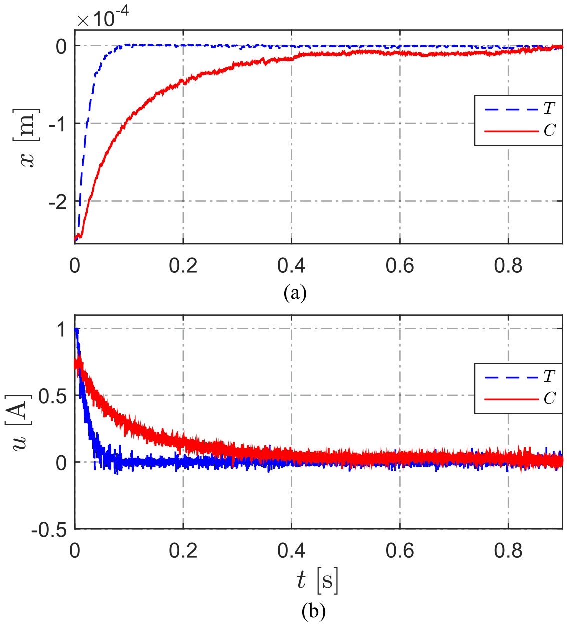

Fig. 11. (a) Evolution of the x-axis control performance and (b) control signal of IT2.

the control signal of C does not reach the saturation value of input constraint whereas the control signal of T meets it at the beginning stage. Therefore, the effectiveness of Corollary 1 on input constraint is thus verified.

VI. Conclusion

In this article, an active IT2 T–S model-based fuzzy levitation control system has been established. In the controller, IT2 fuzzy memberships are deliberately designed to address the complex AMB system uncertainties, whereas the control law via the PDC scheme is designed to overcome both nonlinearities and external disturbances based on the local linearized model. Theoretical analysis has been implemented to derive the stability conditions to guarantee the feasibility of the proposed fuzzy controller. When control input constraints are considered, an additional condition has also been analyzed. Experiments have been conducted to evaluate the advantages of the present IT2 T–S fuzzy controller over the conventional LQR, H_∞, and T1 controllers, in terms of quicker levitation, higher tracking precision, and superior capability of external disturbance rejection. The proposed active IT2 controller has promising potential in AMB rotor applications to a large volume of processes including complex surface machining, vacuum pump antivibration systems, and so on.

Appendix

According to Theorem 1 and using the model dynamics (10) and the system parameters listed in Table I, one can find the matrices P and W for a single axis by the LMI tool of MATLAB as follows:

$$P = \begin{bmatrix} 4.67e7 & 6.46e3 \\ 6.46e3 & 6.03e2 \end{bmatrix}$$

$$W =$$

$$\left[\begin{matrix} 1.40e8 & -8.6e6 & -6.59e8 & -6.30e7 & 0 \\ -8.60e6 & 1.06e6 & -6.30e7 & 4.78e5 & 0 \\ 5.88e8 & 6.33e7 & 2.38e8 & 4.70e6 & -1.83e7 \\ 6.33e7 & -6.18e5 & 4.70e6 & 3.60e5 & -1.35e7 \\ 0 & 0 & 6.53e6 & 1.32e7 & 1.96e8 \\ 0 & 0 & 1.32e7 & -2.29e5 & 2.38e6 \\ 0 & 0 & 0 & 0 & -1.83e7 \\ 0 & 0 & 0 & 0 & -1.35e7 \\ 0 & 0 & 0 & 0 & 0 \\ 0 & 0 & 0 & 0 & 0 \end{matrix}\right.$$

$$\left.\begin{matrix} 0 & 0 & 0 & 0 & 0 \\ 0 & 0 & 0 & 0 & 0 \\ -1.35e7 & 0 & 0 & 0 & 0 \\ 1.63e5 & 0 & 0 & 0 & 0 \\ 2.38e6 & 6.53e6 & 1.32e7 & 0 & 0 \\ -1.35e7 & 2.38e8 & 4.70e6 & 5.88e8 & 6.33e7 \\ 1.63e5 & 4.70e6 & 3.60e5 & 6.33e7 & -6.18e5 \\ 0 & -6.59e8 & -6.30e7 & 1.40e8 & -8.6e6 \\ 0 & -6.30e7 & 4.78e5 & -8.60e6 & 1.06e6 \end{matrix}\right].$$

According to [16], the H_∞ controller of the single-axis AMB used in Section V is calculated as

$$K(s) = \frac{1.06e08\, s^2 + 5.25e10\, s + 3.05e12}{s^3 + 1.11e4s^2 + 1.38e07\, s + 1.38e3}$$

and its discrete-time transfer function, with the sample time $T_s = 0.1$ ms, is

$$K(z) = \frac{3405z^3 - 3239z^2 - 3404z + 3240}{z^3 - 2.214z^2 + 1.514z - 0.3007}.$$

References

[1] G. Schweitzer and E. H. Maslen, *Magnetic Bearings: Theory, Design, and Application to Rotating Machinery*. Berlin, Germany: Springer, 2009.

[2] G. Loussert and J.-D. Alzingre, "A magnetic and mechanical force model for the design of an Archimedean spiral flexure bearing for a linear direct-drive electromagnetic actuator," *IEEE Trans. Mechatronics*, vol. 24, no. 4, pp. 1617–1627, Aug. 2019.

[3] K. Wang, X. Ma, Q. Liu, S. Chen, and X. Liu, "Multiphysics global design and experiment of the electric machine with a flexible rotor supported by active magnetic bearing," *IEEE/ASME Trans. Mechatronics*, vol. 24, no. 2, pp. 820–831, Apr. 2019.

[4] M. O. T. Cole and W. Fakkaew, "An active magnetic bearing for thin-walled rotors: Vibrational dynamics and stabilizing control," *IEEE/ASME Trans. Mechatronics*, vol. 23, no. 6, pp. 2859–2869, Dec. 2018.

[5] Y. Yuan, H.-T. Zhang, Y. Wu, T. Zhu, and H. Ding, "Bayesian learning-based model-predictive vibration control for thin-walled workpiece machining processes," *IEEE/ASME Trans. Mechatronics*, vol. 22, no. 1, pp. 509–520, Feb. 2017.

[6] B. Xiang and W. Wong, "Vibration characteristics analysis of magnetically suspended rotor in flywheel energy storage system," *J. Sound Vib.*, vol. 444, no. 3, pp. 235–247, 2019.

[7] L. Zhang, J. Du, and J. Feng, "Control for the magnetically suspended flat rotor tilting by axial forces in a small-scale control moment gyro," *IEEE Trans. Ind. Electron.*, vol. 65, no. 3, pp. 2449–2457, Mar. 2018.

[8] H.-T. Zhang, P. Chen, X. Zhang, and H. Ding, "Saturated output regulation approach for active vibration control of thin-walled flexible workpieces with voice coil actuators," *IEEE/ASME Trans. Mechatronics*, vol. 21, no. 1, pp. 266–275, Feb. 2016.

[9] S. M. Yang and M. S. Huang, "Design and implementation of a magnetically levitated single-axis controlled axial blood pump," *IEEE Trans. Ind. Electron.*, vol. 56, no. 6, pp. 2213–2219, Jun. 2009.

[10] J. Sun and H. Ren, "Design and analysis of magnetic suspension actuators in medical robotics," in *Proc. Electromagn. Actuation Sens. Med. Robot.*, 2018, pp. 105–139.

[11] S. E. Mushi, Z. Lin, and P. E. Allaire, "Design, construction, and modeling of a flexible rotor active magnetic bearing test rig," *IEEE/ASME Trans. Mechatronics*, vol. 17, no. 6, pp. 1170–1182, Dec. 2012.

[12] A. M. Benomair, F. A. Bashir, and M. O. Tokhi, "Optimal control based LQR-feedback linearisation for magnetic levitation using improved spiral dynamic algorithm," in *Proc. 20th Int. Conf. Methods Models Autom. Robot.*, 2015, pp. 558–562.

[13] Y. Wu, G.-P. Ren, and H.-T. Zhang, "Dual-mode predictive control of a rotor suspension system," *Sci. China Inf. Sci.*, vol. 63, no. 1, 2020, Art. no. 112204.

[14] T. Du, Y. Sun, H. Geng, Y. Li, H. Lv, and L. Yu, "Dynamic analysis on rotor system supported by active magnetic bearings based on sliding mode control," in *Proc. IEEE Int. Conf. Mechatronics Autom.*, 2018, pp. 1960–1965.

[15] H. Balini, C. W. Scherer, and J. Witte, "Performance enhancement for AMB systems using unstable H_∞ controllers," *IEEE Trans. Control Syst. Technol.*, vol. 19, no. 6, pp. 1479–1492, Nov. 2011.

[16] S. S. Nair, "Automatic weight selection algorithm for designing H_∞ controller for active magnetic bearing," *Int. J. Eng. Sci. Technol.*, vol. 3, no. 1, pp. 122–138, 2011.

[17] C. Liu, G. Liu, and J. Fang, "Feedback linearization and extended state observer-based control for rotor-AMBs system with mismatched uncertainties," *IEEE Trans. Ind. Electron.*, vol. 64, no. 2, pp. 1313–1322, Feb. 2017.

[18] A. Pesch and J. Sawicki, "Active magnetic bearing online levitation recovery through μ-synthesis robust control," *Actuators*, vol. 6, no. 1, 2017, Art. no. 2.

[19] P. R. Ouyang, W. J. Zhang, and M. M. Gupta, "An adaptive switching learning control method for trajectory tracking of robot manipulators," *Mechatronics*, vol. 16, no. 1, pp. 51–61, 2006.

[20] Y. Yuan *et al.*, "Data driven discovery of cyber physical systems," *Nature Commun.*, vol. 10, no. 1, pp. 1–9, 2019.

[21] Y. Yuan *et al.*, "A general end-to-end diagnosis framework for manufacturing systems," *Nat. Sci. Rev.*, Nov. 2019, doi: 10.1093/nsr/nwz190.

[22] M. S. Kandil, M. R. Dubois, L. S. Bakay, and J. P. F. Trovao, "Application of second-order sliding-mode concepts to active magnetic bearings," *IEEE Trans. Ind. Electron.*, vol. 65, no. 1, pp. 855–864, Jan. 2018.

[23] T. Schuhmann, W. Hofmann, and R. Werner, "Improving operational performance of active magnetic bearings using Kalman filter and state feedback control," *IEEE Trans. Ind. Electron.*, vol. 59, no. 2, pp. 821–829, Feb. 2012.

[24] T. Takagi and M. Sugeno, "Fuzzy identification of systems and its applications to modeling and control," *IEEE Trans. Syst., Man, Cybern.*, vol. SMC-15, no. 1, pp. 116–132, Jan./Feb. 1985.

[25] D. Wang and F. Wang, "Design of PDC controller based on TS fuzzy model for magnetic bearing of high-speed motors," in *Proc. 3rd Int. Conf. Comput. Sci. Inf. Technol.*, 2010, vol. 1, pp. 602–606.

[26] A. S. Reddy, P. K. Agarwal, and S. Chand, "Adaptive multipopulation genetic algorithm based self designed fuzzy logic controller for active magnetic bearing application," *Int. J. Dyn. Control*, vol. 6, no. 3, pp. 1392–1408, 2018.

[27] A. Dhyani, M. K. Panda, and B. Jha, "Moth-flame optimization-based fuzzy-PID controller for optimal control of active magnetic bearing system," *Iranian J. Sci. Technol., Trans. Elect. Eng.*, vol. 42, no. 4, pp. 451–463, 2018.

[28] H. Zhou and H. Ying, "Deriving and analyzing analytical structures of a class of typical interval type-2 TS fuzzy controllers," *IEEE Trans. Cybern.*, vol. 47, no. 9, pp. 2492–2503, Sep. 2017.

[29] O. Castillo and K. Atanassov, "Comments on fuzzy sets, interval type-2 fuzzy sets, general type-2 fuzzy sets and intuitionistic fuzzy sets," in *Proc. Recent Adv. Intuitionistic Fuzzy Logic Syst.*, 2019, pp. 35–43.

[30] D. Wu and J. M. Mendel, "Recommendations on designing practical interval type-2 fuzzy systems," *Eng. Appl. Artif. Intell.*, vol. 85, pp. 182–193, 2019.

[31] J. Huang, M. Ri, D. Wu and S. Ri, "Interval type-2 fuzzy logic modeling and control of a mobile two-wheeled inverted pendulum," *IEEE Trans. Fuzzy Syst.*, vol. 26, no. 4, pp. 2030–2038, Aug. 2018.

[32] S. Hassan, A. Khosravi, J. Jaafar, and M. A. Khanesar, "A systematic design of interval type-2 fuzzy logic system using extreme learning machine for electricity load demand forecasting," *Int. J. Elect. Power Energy Syst.*, vol. 82, pp. 1–10, 2016.

[33] J.-Y. Jhang, C.-J. Lin, C.-T. Lin, and K.-Y. Young, "Navigation control of mobile robots using an interval type-2 fuzzy controller based on dynamic-group particle swarm optimization," *Int. J. Control, Autom. Syst.*, vol. 16, no. 5, pp. 2446–2457, 2018.

[34] A. Al-Mahturi, F. Santoso, M. A. Garratt, and S. G. Anavatti, "An intelligent control of an inverted pendulum based on an adaptive interval type-2 fuzzy inference system," in *Proc. IEEE Int. Conf. Fuzzy Syst.*, 2019, pp. 1–6.

[35] H. K. Khalil and J. W. Grizzle, *Nonlinear Systems*. Upper Saddle River, NJ, USA: Prentice-Hall, 2002.

[36] S. M. Darbandi, M. Behzad, H. Salarieh, and H. Mehdigholi, "Linear output feedback control of a three-pole magnetic bearing," *IEEE/ASME Trans. Mechatronics*, vol. 19, no. 4, pp. 1323–1330, Aug. 2014.

[37] H.-Y. Kim and C.-W. Lee, "Design and control of active magnetic bearing system with Lorentz force-type axial actuator," *Mechatronics*, vol. 16, no. 1, pp. 13–20, 2006.

[38] K. Tanaka and H. O. Wang, *Fuzzy Control Systems Design and Analysis: A Linear Matrix Inequality Approach*. Hoboken, NJ, USA: Wiley, 2004.

[39] H. K. Lam and L. D. Seneviratne, "Stability analysis of interval type-2 fuzzy-model-based control systems," *IEEE Trans. Syst., Man, Cybern. B, Cybern.*, vol. 38, no. 3, pp. 617–628, Jun. 2008.

[40] M. Nie and W. W. Tan, "Towards an efficient type-reduction method for interval type-2 fuzzy logic systems," in *Proc. IEEE Int. Conf. Fuzzy Syst.*, 2008, pp. 1424–1432.

[41] D. Wu, "Approaches for reducing the computational cost of interval type-2 fuzzy logic systems: overview and comparisons," *IEEE Trans. Fuzzy Syst.*, vol. 21, no. 1, pp. 80–99, Feb. 2013.

[42] D. Wu, "On the fundamental differences between interval type-2 and type-1 fuzzy logic controllers," *IEEE Trans. Fuzzy Syst.*, vol. 20, no. 5, pp. 832–848, Oct. 2012.

[43] K. Tanaka, T. Ikeda, and H. O. Wang, "Robust stabilization of a class of uncertain nonlinear systems via fuzzy control: Quadratic stabilizability, H_∞ control theory, and linear matrix inequalities," *IEEE Trans. Fuzzy Syst.*, vol. 4, no. 1, pp. 1–13, Feb. 1996.

[44] R. A. Horn and C. R. Johnson. *Matrix Analysis*. Cambridge, U.K.: Cambridge Univ. Press, 2012.

Gui-Ping Ren (Student Member, IEEE) received the B.E. degree in control science and engineering from the School of Automation, Huazhong University of Science and technology (HUST), Wuhan, China, in 2016, where he is currently working toward the Ph.D. degree, majoring in control science and engineering.

His research interests include design, analysis, and control of intelligent mechanical systems.

Zhiyong Chen (Senior Member, IEEE) received the B.E. degree in automatic control from the University of Science and Technology of China, Hefei, China, in 2000, and the M.Phil. and Ph.D. degrees from the Chinese University of Hong Kong, Hong Kong, in 2002 and 2005, respectively, both in mechanical engineering.

From 2005 to 2006, he was a Research Associate with the University of Virginia, Charlottesville, VA, USA. In 2006, he joined the University of Newcastle, Callaghan, NSW, Australia, where he is currently a Professor. He is also a Changjiang Chair Professor with Central South University, Changsha, China. His research interests include nonlinear systems and control, biological systems, and multiagent systems.

Prof. Chen is/was an Associate Editor for *Automatica*, the IEEE TRANSACTIONS ON AUTOMATIC CONTROL, and IEEE TRANSACTIONS ON CYBERNETICS.

Hai-Tao Zhang (Senior Member, IEEE) received the B.E. and Ph.D. degrees from the University of Science and Technology of China, Hefei, China, in 2000 and 2005, respectively, both in automatic control.

During January to December 2007, he was a Postdoctoral Researcher with the University of Cambridge, Cambridge, U.K. Since 2005, he has been with the Huazhong University of Science and Technology, Wuhan, China, where he was an Associate Professor from 2005 to 2010 and has been a Full Professor since 2010. He is currently a Cheung Kong Young Scholar. His research interests include swarming intelligence, model predictive control, and unmanned system cooperation control.

Dr. Zhang is/was an Associate Editor for the IEEE TRANSACTIONS ON CIRCUITS AND SYSTEMS II and *Asian Journal of Control*.

Yue Wu (Member, IEEE) received the Ph.D. degree in automatic control from the School of Automation, Huazhong University of Science and Technology (HUST), Wuhan, China, in 2017.

He is currently working toward the Postdoctoral Researcher of Mechatronics with the School of Mechanical Science and Engineering, HUST. His research interests include active chatter mitigation control, adaptive control, and model predictive control.

Dr. Wu was the recipient of the Outstanding Reviewer Award of the *Asian Journal of Control* in 2015.

Haofei Meng received the B.E. degree from the Wuhan University of Technology, Wuhan, China, in 2010, the M.E. degree of control theory and engineering from the University of Science and Technology of China, Hefei, China, in 2013, and the Ph.D. degree in electrical engineering from the University of Newcastle, Callaghan, NSW, Australia, in 2017.

She is currently working toward the Postdoctoral Researcher in Control Theory and Engineering with the School of Artificial Intelligence and Automation, Huazhong University of Science and Technology, Wuhan, China. Her research interests include multiagent systems, time-delay systems, and switched systems.

Dongrui Wu (Senior Member, IEEE) received the B.E. degree in automatic control from the University of Science and Technology of China, Hefei, China, in 2003, the M.E. degree in electrical engineering from the National University of Singapore, Singapore, in 2005, and the Ph.D. degree in electrical engineering from the University of Southern California, Los Angeles, CA, USA, in 2009.

He is currently a Professor with the School of Artificial Intelligence and Automation, Huazhong University of Science and Technology, Wuhan, China, and Deputy Director of the Key Laboratory of Image Processing and Intelligent Control, Ministry of Education. He has authored or coauthored more than 140 publications, including a book entitled *Perceptual Computing* (Wiley-IEEE Press, 2010). His research interests include affective computing, brain–computer interfaces, computational intelligence, and machine learning.

Dr. Wu was the recipient of the IEEE Computational Intelligence Society Outstanding Ph.D. Dissertation Award in 2012, the IEEE TRANSACTIONS ON FUZZY SYSTEMS Outstanding Paper Award in 2014, the North America Fuzzy Information Processing Society (NAFIPS) Early Career Award in 2014, the IEEE Systems, Man, and Cybernetics (SMC) Society Early Career Award in 2017, and the IEEE SMC Society Best Associate Editor Award in 2018. He was also a finalist for three other best paper awards. He was/is an Associate Editor for the IEEE TRANSACTIONS ON FUZZY SYSTEMS (2011–2018), IEEE TRANSACTIONS ON HUMAN–MACHINE SYSTEMS (since 2014), *IEEE Computational Intelligence Magazine* (since 2017), and IEEE TRANSACTIONS ON NEURAL SYSTEMS AND REHABILITATION ENGINEERING (since 2019).

Han Ding (Senior Member, IEEE) received the Ph.D. degree in mechatronics from the Huazhong University of Science and Technology (HUST), Wuhan, China, in 1989.

He was with the University of Stuttgart, Stuttgart, Germany, in 1993, supported by the Alexander von Humboldt Foundation. He is currently the Chairman of the Academic Committee of HUST and the Director of the National Innovation Institute of Digital Design and Manufacturing, and is also the Leader of Steering Expert Group of the NSFC Tri-Co Robot major research program. He has long dedicated himself to research in the field of robotics and digital manufacturing, and has successfully combined both technologies. He is the author coauthor of three academic books and more than 300 journal papers, and licensed more than 60 patents in China.

Prof. Ding was the recipient of the National Distinguished Youth Scientific Fund in 1997 and the "Cheung Kong" Chair Professor at Shanghai Jiao Tong University in 2001. He was an Associate Editor for the IEEE TRANSACTIONS ON AUTOMATION SCIENCE AND ENGINEERING (TASE) from 2004 to 2007. He is currently a Senior Editor for the *IEEE Robotics and Automation Letters*. He was elected a Member of the Chinese Academy of Sciences in 2013.